The Plant Cell, Vol. 11, 1081–1092, June 1999, www.plantcell.org © 1999 American Society of Plant Physiologists

Structure of a Plant Cell Wall Fragment Complexed to Pectate Lyase C

Robert D. Scavetta,[a,1] Steven R. Herron,[a] Arland T. Hotchkiss,[b] Nobuhiro Kita,[a,2] Noel T. Keen,[c] Jacques A. E. Benen,[d] Harry C. M. Kester,[d] Jaap Visser,[d] and Frances Jurnak[a,3]

[a] Department of Physiology and Biophysics, 346-D Med Sci I, University of California, Irvine, California 92697-4560
[b] U.S. Department of Agriculture–Agricultural Research Service, Eastern Regional Research Center, 600 E. Mermaid Lane, Wyndmoor, Pennsylvania 19038-8598
[c] Department of Plant Pathology, University of California, Riverside, California 92521
[d] Department of Molecular Genetics of Industrial Microorganisms, Wageningen Agricultural University, Dreijenlaan 2, 6703 HA Wageningen, The Netherlands

The three-dimensional structure of a complex between the pectate lyase C (PelC) R218K mutant and a plant cell wall fragment has been determined by x-ray diffraction techniques to a resolution of 2.2 Å and refined to a crystallographic *R* factor of 18.6%. The oligosaccharide substrate, α-D-Gal*p*A-([1→4]-α-D-Gal*p*A)$_3$-(1→4)-D-Gal*p*A, is composed of five galacturonopyranose units (D-Gal*p*A) linked by α-(1→4) glycosidic bonds. PelC is secreted by the plant pathogen *Erwinia chrysanthemi* and degrades the pectate component of plant cell walls in soft rot diseases. The substrate has been trapped in crystals by using the inactive R218K mutant. Four of the five saccharide units of the substrate are well ordered and represent an atomic view of the pectate component in plant cell walls. The conformation of the pectate fragment is a mix of 2_1 and 3_1 right-handed helices. The substrate binds in a cleft, interacting primarily with positively charged groups: either lysine or arginine amino acids on PelC or the four Ca^{2+} ions found in the complex. The observed protein–oligosaccharide interactions provide a functional explanation for many of the invariant and conserved amino acids in the pectate lyase family of proteins. Because the R218K PelC–galacturonopentaose complex represents an intermediate in the reaction pathway, the structure also reveals important details regarding the enzymatic mechanism. Notably, the results suggest that an arginine, which is invariant in the pectate lyase superfamily, is the amino acid that initiates proton abstraction during the β elimination cleavage of polygalacturonic acid.

INTRODUCTION

Pectate lyases are depolymerizing enzymes that degrade plant cell walls, causing tissue maceration and death. The enzymes normally are secreted by phytopathogenic organisms and are known to be the primary virulence agents in soft rot diseases caused by *Erwinia* spp (Collmer and Keen, 1986; Kotoujansky, 1987; Barras et al., 1994). In the latter organisms, the enzymes exist as multiple, independently regulated isozymes that share amino acid sequence identity ranging from 27 to 80%.

Pectate lyases share sequence similarities with fungal pectin lyases, plant pollen proteins, and plant style proteins (Henrissat et al., 1996). The three-dimensional structures of five members of the superfamily have been determined and include *Erwinia chrysanthemi* pectate lyase C (PelC) (Yoder et al., 1993; Yoder and Jurnak, 1995), *E. chrysanthemi* pectate lyase E (PelE) (Lietzke et al., 1994), *Bacillus subtilis* pectate lyase (*B. subtilis* Pel) (Pickersgill et al., 1994), *Aspergillus niger* pectin lyase A (PLA) (Mayans et al., 1997), and *A. niger* pectin lyase B (PLB) (Vitali et al., 1998). All share a similar but an unusual structural motif, termed the parallel β helix, in which the β strands are folded into a large, right-handed coil. The enzyme structures differ in the size and conformation of the loops that protrude from the parallel β helix core. As deduced from sequence similarity and site-directed mutagenesis studies, the protruding loops on one side of the parallel β helix form the pectolytic active site (Kita et al., 1996). The structural differences of the loops are believed to be related to subtle differences in the enzymatic and maceration properties of the proteins.

Pectate lyases catalyze the cleavage of pectate, the de-esterified product of pectin, which is the major component that maintains the structural integrity of cell walls in higher plants

[1] Current address: 6803 South Ivy Way, Inglewood, CO 80112.
[2] Current address: Kanagawa Institute of Agricultural Science, 1617 Kamikisawa, Hiratsuka, Kanagawa 259-12, Japan.
[3] To whom correspondence should be addressed. E-mail jurnak@uci.edu; fax 949-824-8540.

(Carpita and Gibeaut, 1993). The pectate backbone is composed of blocks of polygalacturonic acid (PGA), which is a helical homopolymer of D-galacturonic acid (Gal*p*A) units linked by α-(1→4) glycosidic bonds. The blocks of PGA are separated by stretches in which (1→2)-α-L-rhamnose residues alternate with Gal*p*A (McNaught, 1997). Blocks of PGA may contain as many as 200 Gal*p*A units and span 100 nm (Thibault et al., 1993). Cations are necessary to neutralize PGA in solution and, as a consequence, influence its structure.

In the presence of Ca^{2+}, PGA assumes a 2_1 helical conformation in dilute polymer concentrations (Morris et al., 1982; Powell et al., 1982) and a 3_1 helix at high concentrations in either a gel or solid form (Walkinshaw and Arnott, 1981a, 1981b). Because the PGA concentration in the plant cell wall upon demethylation of pectin lies near the critical conformational transition point, considerable speculation exists as to the in situ structure of PGA. A popular view is the "eggbox model" in which Ca^{2+} ions cross-link the uronic acid moieties of neighboring antiparallel chains of PGA together. Although the eggbox model generally is depicted with PGA in a right-handed 2_1 helical conformation, the original literature suggests that cross-linking between Ca^{2+} and PGA in a right- or left-handed 3_1 helical conformation is feasible as well (Grant et al., 1973; Kohn, 1975).

The results of a recent nuclear magnetic resonance study suggest that the Ca^{2+}–PGA complex in the plant cell wall is much more complex than the simple eggbox model. This complex contains both 2_1 and 3_1 helices of PGA as well as intermediate conformational states (Jarvis and Apperley, 1995). Nuclear magnetic resonance, molecular modeling, and molecular dynamic analyses of pectic disaccharides and trisaccharides also have reported that PGA has both 3_1 and 2_1 helical conformations (Hricovini et al., 1991; DiNola et al., 1994; Gouvion et al., 1994). Disaccharide hydration and sodium salt formation may shift the predicted PGA helical conformation from 3_1 to 2_1 (DiNola et al., 1994; Gouvion et al., 1994; Catoire et al., 1997).

All proteins in the pectate lyase superfamily are believed to share a similar enzymatic mechanism, but the catalytic roles of the amino acids in the active site region have not been identified. For reasons of technical convenience, recent studies have focused on PelC. The enzyme randomly cleaves PGA by a β elimination mechanism, generating primarily a trimer end product with a 4,5-unsaturated bond in the galacturonosyl residue (α-L-4-eno-threohexosylpyranosyluronic acid [α-L-4-en-thrHex*p*A]) at the nonreducing end (Preston et al., 1992). PelC has an in vitro pH optimum of 9.5 and requires Ca^{2+} for pectolytic activity. Structural studies

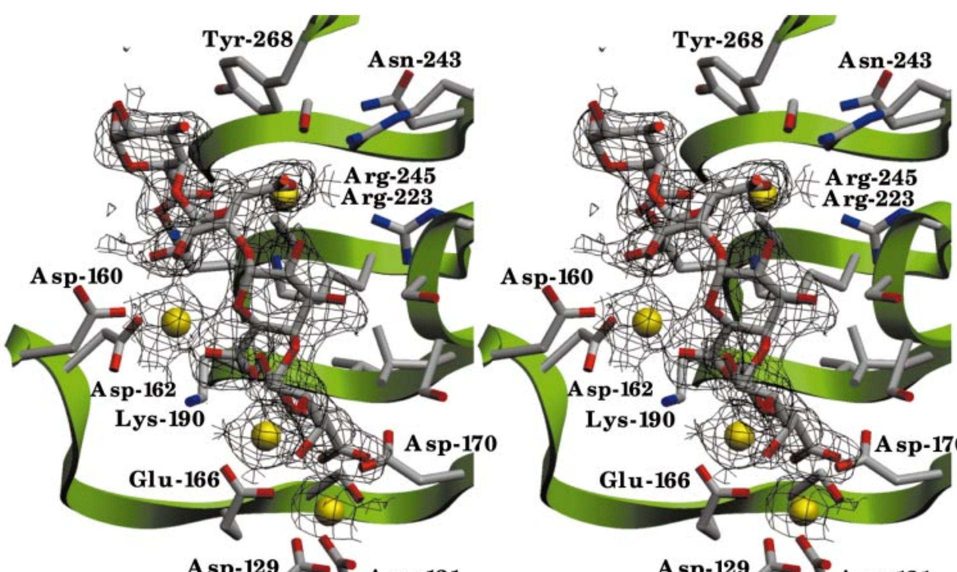

Figure 1. Stereoview of the Ca^{2+} Ions and TetraGal*p*A Superimposed upon the Simulated Annealed OMIT Electron Density Map of the PelC R218K–Substrate Complex Contoured at 1.0σ.

The Ca^{2+} ions are represented by yellow spheres. TetraGal*p*A as well as the interacting amino acids are represented by rods by using the International Union of Pure and Applied Chemistry coloring code: carbon atoms are gray; oxygen atoms, red; and nitrogen atoms, blue. The R218K backbone is represented by green ribbons. Individual amino acids that are shown are labeled at the α-carbon.

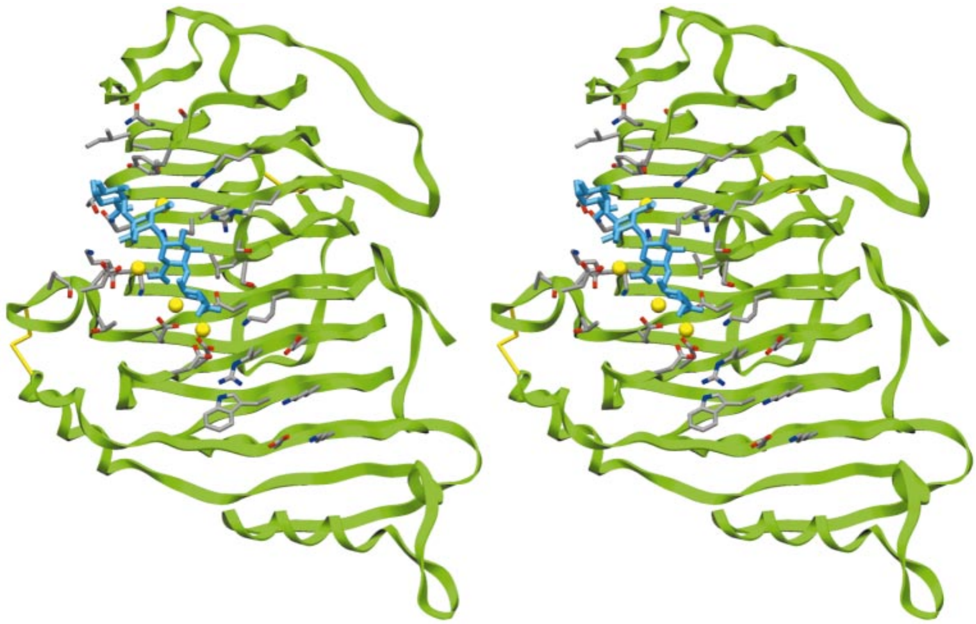

Figure 2. Stereoview of the PelC R218K–$(Ca^{2+})_{3–4}$–PentaGal*p*A Complex.

The view and color scheme are the same as given in Figure 1, except that the tetraGal*p*A substrate is illustrated in cyan, the entire protein backbone is shown, and the individual amino acids are not labeled. The disulfide bonds are illustrated as yellow rods.

have shown that Ca^{2+} is bound to the enzyme at a location that was first suggested in a PelC–Lu^{3+} complex (Yoder et al., 1993) and later confirmed by structural studies of a *B. subtilis* Pel–Ca^{2+} complex (Pickersgill et al., 1994). The role of Ca^{2+} has not been established. In the β elimination reaction, the reaction is initiated by proton abstraction from C-5 of the galacturonosyl residue on the reducing side of the glycosidic scissile bond. The group or groups that initiate proton abstraction and transfer the proton to the glycosidic oxygen have not been identified. Potential candidates include two invariant amino acids in the superfamily, Asp-131 and Arg-218 in PelC nomenclature, as well as four amino acids, Glu-166, Asp-170, Lys-190, and Arg-223, which are invariant within the pectate lyase subfamily (Henrissat et al., 1996). Site-specific mutations at the latter PelC positions abolish pectolytic as well as maceration activity (Kita et al., 1996). Notably, the pectolytic region is devoid of conserved histidine, serine, or tyrosine residues, which frequently are implicated in β elimination enzymatic mechanisms with a lower pH optimum. In this study, we have taken advantage of the impaired catalytic properties of one PelC mutant, R218K, to form a stable substrate–enzyme complex that could be studied by x-ray diffraction techniques. The results provide an atomic view of a pectate fragment, α-D-Gal*p*A-([1→4]-α-D-Gal*p*A)$_3$-(1→4)-D-Gal*p*A (pentaGal*p*A), and the identification of the key amino acids involved in oligosaccharide binding. In addition, the results provide tentative identification of the amino acid that initiates proton abstraction.

RESULTS

Conformation of the PentaGal*p*A Substrate

Four of the five Gal*p*A units of the substrate used in the crystal diffusion experiment are visible as strong, well-ordered electron density in difference Fourier maps, as shown in Figure 1. As shown in Figure 2, the well-ordered Gal*p*A units interact with PelC in a groove encompassing the previously identified Ca^{2+} binding site on the protein, now termed the $^4Ca^{2+}$ site. The orientation of the tetraGal*p*A fragment is unambiguous. The reducing end, Gal*p*A^1, is located at the protein–solvent border, and the nonreducing end, Gal*p*A^4, lies near $^4Ca^{2+}$. Additional electron density, corresponding to a fifth Gal*p*A unit, is found at the nonreducing end of the tetraGal*p*A fragment but is disordered and cannot be modeled.

Each of the well-ordered Gal*p*A rings refines to the conventional chair conformation, with all bond distances and angles consistent with single bonds. The pectate fragment

Table 1. Bond Angles (τ) and Torsional Rotations (ϕ and ψ) about Glycosidic Bonds in the Refined Structures of the PelC–$(Ca^{2+})_{3-4}$–PentaGal*p*A Complexes[a]

Glycosidic Bond	τ[b]	ϕ[c]	ψ[d]
3_1 Helix[e]	117.0°	80.0°	89.0°
2_1 Helix[f]	117.0°	80.0°	161.0°
Gal*p*A[1]–Gal*p*A[2]	117.0°	54.0°	90.0°
Gal*p*A[2]–Gal*p*A[3]	116.6°	117.0°	157.0°
Gal*p*A[3]–Gal*p*A[4]	120.4°	73.0°	51.0°

[a] Torsional angles were determined by looking from the nonreducing end side (with prime) down the bond of interest to the reducing end side and determining the angle of rotation created from the planes of O-5′–C-1′–O-4 and C-1′–O-4–C-4 for ϕ and C-1′–O-4–C-4 and O-4–C-4–C-5 for ψ. A *cis* configuration is taken to be 0°, and a *trans* configuration is taken to be 180°. A negative sign is a rotation from *cis* in a counterclockwise direction, and a positive sign is a rotation from *cis* in a clockwise direction.
[b] τ, the C_1–O–$C_4{}'$ bond angle.
[c] ϕ, the torsional rotation about the C_1–O bond.
[d] ψ, the torsional rotation about the O–$C_4{}'$ bond.
[e] The values for the 3_1 helix are those determined by the program O (Jones et al., 1991) from the model published by Walkinshaw and Arnott (1981b).
[f] The values for the 2_1 helix are those determined by the program O for a galacturonic acid model constructed using the parameters for alginic acid by Atkins et al. (1973).

folds into an unbent right-handed helical conformation, with the observed helical angles compared with the idealized 2_1 and 3_1 helices in Table 1. Two of the three glycosidic bonds have ψ torsional angles that approximate the 3_1 helix observed in fiber diffraction studies of PGA–Ca^{2+} gels (Walkinshaw and Arnott, 1981a, 1981b). One of the glycosidic bonds, between Gal*p*A[2] and Gal*p*A[3], has a ψ torsional angle similar to a 2_1 helix. Consequently, the overall appearance of the pectate fragment conformation is of a 3_1 helix, but with the middle segment distorted into 2_1 helix, as illustrated in Figures 3A and 3B. Given the greater number of Gal*p*A[3] contacts, as listed in Table 2, the deviation from the 3_1 helical conformation is probably a result of specific interactions with the enzyme. The deviation is not likely due to other effects, such as pectate concentration, hydration, or cation type, which are postulated to cause the transition between 2_1 and 3_1 helical conformations of pectate. If the R218K–$(Ca^{2+})_{3-4}$–Gal*p*A_5 structures are representative of interactions that occur within the plant cell wall, then endogenous proteins also are likely to distort the PGA conformation from any helical states observed under in vitro conditions.

Coordination of Ca^{2+} Ions

In wild-type PelC, a Ca^{2+} ion coordinates to seven ligands, including two water molecules, both carboxyl oxygens of Asp-131, and one carboxyl oxygen from each of Asp-129, Glu-166, and Asp-170. In the R218K complex with pentaGal*p*A, the equivalent $^4Ca^{2+}$ coordinates to the same groups, with a single exception—a carboxyl oxygen from Gal*p*A[4] replaces one of the water molecules. In addition to $^4Ca^{2+}$, three additional Ca^{2+} ions have been identified. Two of the additional Ca^{2+} ions, $^2Ca^{2+}$ and $^3Ca^{2+}$, are fully occupied, and the third, $^1Ca^{2+}$, has a partial occupancy of ∼50%. Each Ca^{2+} ion bridges the carboxyl group of each Gal*p*A unit to the protein. In addition, $^2Ca^{2+}$ and $^3Ca^{2+}$ link the uronic acid moieties of Gal*p*A[2], Gal*p*A[3], and Gal*p*A[4]. The coordination around each Ca^{2+} ion is listed in Table 3. The observed Ca^{2+} positions are very different from the interstrand Ca^{2+} ions

Table 2. Atomic Distances of 3.0 Å or Less between the Oxygen Atoms of TetraGal*p*A and Amino Acids, Ca^{2+} Ions, or Water Molecules

Gal*p*A Atoms[a]	Interacting Atoms[b]	Distance (Å)
Gal*p*A[1]		
Ring interaction	Tyr-268	
O-6A	$^{GA1}Wat^1$	2.9
O-6B	$^1Ca^{2+}$	2.9
Gal*p*A[2]		
O-2	Asp-162 O-δ2	2.7
O-2	$^{GA2}Wat^1$	2.7
O-3	$^2Ca^{2+}$	2.6
O-5	$^1Ca^{2+}$	2.9
O-6A	$^1Ca^{2+}$	2.6
O-6A	Arg-245 NH-1	2.8
O-6B	Arg-245 NH-2	3.0
O-6B	$^{GA2}Wat^2$	2.8
Gal*p*A[3]		
O-2	Arg-223 NH-2	2.9
O-3	Ser-196 O	2.8
O-3	Arg-223 NH-1	2.9
O-5	$^2Ca^{2+}$	2.5
O-5	$^{2Ca}Wat^2$	3.0
O-6A	Lys-190 N-ζ	2.8
O-6A	$^2Ca^{2+}$	2.3
O-6A	$^{2Ca}Wat^2$	2.9
O-6B	$^3Ca^{2+}$	2.4
O-6B	$^{3Ca}Wat^3$	2.8
Gal*p*A[4]		
O-2	$^{2Ca}Wat^2$	2.9
O-3	$^{GA4}Wat^1$	2.8
O-4	$^{GA4}Wat^2$	2.7
O-4	Ser-308 O	2.8
O-5	$^3Ca^{2+}$	2.4
O-6A	$^4Ca^{2+}$	2.5
O-6A	$^3Ca^{2+}$	2.4
O-6A	$^{GA4}Wat^2$	2.9
O-6B	$^{4Ca}Wat^1$	2.6

[a] The positions of the atoms are indicated in Figure 4.
[b] $^xWat^y$ refers to the Y water molecule associated with the X Gal*p*A unit. $^zCa^{2+}$ refers to the Z position of the Ca^{2+} ion as defined in Figure 4.

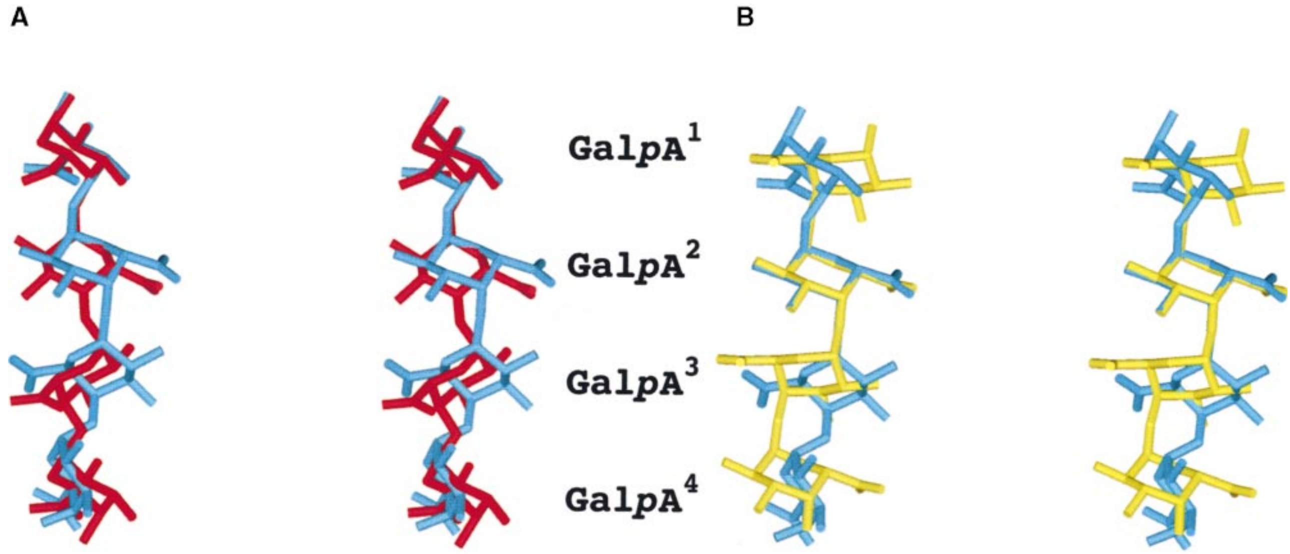

Figure 3. Stereoview of the TetraGal*p*A Structure Superimposed upon Modeled Right-Hand 2_1 and 3_1 OligoGal*p*A Helices.

The tetraGal*p*A structure determined at 2.2 Å is shown in both **(A)** and **(B)** as cyan rods.

(A) The modeled 3_1 oligoGal*p*A helix (Walkinshaw and Arnott, 1981a) is shown in red.

(B) The modeled 2_1 oligoGal*p*A helix (Atkins et al., 1973) is shown in yellow.

postulated to link PGA helices together (Walkinshaw and Arnott, 1981a, 1981b; Morris et al., 1982; Powell et al., 1982). In the present structure, the Ca^{2+} ions link not only the oligosaccharide to the protein but also adjacent uronic acid moieties within a single pectate strand.

Protein–Ca^{2+}–TetraGal*p*A Interactions

The protein–Ca^{2+}–tetraGal*p*A interactions are represented in Figure 4, and all relevant interatomic distances are summarized in Table 2. Electrostatic interactions dominate, with the negatively charged uronic acid moieties primarily interacting with positively charged groups: either lysine or arginine on PelC or the four Ca^{2+} ions found in the complex. The carboxyl oxygens of Gal*p*A^2 and Gal*p*A^3 interact strongly with Arg-245 and Lys-190, respectively, whereas a carboxyl oxygen of Gal*p*A^4, at a distance of 3.2 Å from Lys-172, forms a weaker interaction. Lys-172 is highly conserved, and Lys-190 is invariant in the pectate lyases, but neither amino acid is found among the pectin lyases that bind a neutral methylated form of pectate. Arg-245 is conserved only among PelC subfamily members but not in the PelE subfamily whose members rapidly cleave the substrate to an unsaturated dimer. Several additional interactions between tetraGal*p*A and the protein were observed, but notably, the most specific ones involve Gal*p*A^3. Arg-223, another invariant amino acid in the pectate lyase subfamily, forms hydrogen bonds with the C-2 and C-3 hydroxyl groups of Gal*p*A^3, the orientation of which partially defines the galactose epimer. The C-3 hydroxyl group also forms a hydrogen bond with a nonconserved Ser-196. In Gal*p*A^2, the C-2 hydroxyl interacts with Asp-162, and in Gal*p*A^1, the ring forms a stacking interaction with Tyr-268. Both amino acids are conserved but only in the PelC subfamily. In addition to interactions with the protein and Ca^{2+} ions, the tetraGal*p*A segment is highly solvated, forming many hydrogen bonds with water molecules that increase in frequency from Gal*p*A^1 to Gal*p*A^4. Collectively, the observed protein–tetraGal*p*A interactions provide a functional role for all invariant and conserved amino acids in the pectolytic region of the pectate lyases, except one, Arg-218.

Position of Scissile Bond

Crystals of wild-type PelC, which are isomorphous with R218K crystals, cleave pentaGal*p*A when diffused into crystals. Because the R218K mutant is catalytically inactive and a saturated tetraGal*p*A has been observed, the R218K–$(Ca^{2+})_{3-4}$–Gal*p*A_5 complexes represent a Michaelis complex in the reaction pathway. Can the scissile glycosidic bond be identified with certainty? PelC and subfamily members have been reported to cleave a pectate substrate, yielding a trimer as the primary unsaturated end product (68 to 72%; Preston et al., 1992). In the crystal structure, an unsaturated trimeric end product would result only if the scissile bond

Table 3. Ca^{2+}-Coordinating Ligands[a] in the PelC R218K–$(Ca^{2+})_{3–4}$–PentaGal*p*A Complexes

Ca^{2+}	Ligand	Distance (Å)
$^{1}Ca^{2+}$ [b]	Lys-218 N-ζ	2.6
	Gal*p*A[1] O-6B	2.9
	Gal*p*A[2] O-5	2.9
	Gal*p*A[2] O-6A	2.6
	$^{1Ca}Wat^{1}$	2.8
$^{2}Ca^{2+}$	Asp-160 O-δ2	2.3
	Asp-162 O-δ2	2.4
	Gal*p*A[2] O-3	2.6
	Gal*p*A[3] O-5	2.5
	Gal*p*A[3] O-6A	2.2
	$^{2Ca}Wat^{1}$	2.6
	$^{2Ca}Wat^{2}$	2.2
$^{3}Ca^{2+}$	Glu-166 O-δ1	2.5
	Glu-166 O-δ2	2.5
	Gal*p*A[3] O-6B	2.4
	Gal*p*A[4] O-5	2.4
	Gal*p*A[4] O-6A	2.4
	$^{3Ca}Wat^{1}$	2.5
	$^{3Ca}Wat^{2}$	2.4
	$^{3Ca}Wat^{3}$	2.4
$^{4}Ca^{2+}$	Asp-129 O-δ1	2.3
	Asp-131 O-δ1	2.5
	Asp-131 O-δ2	2.4
	Glu-166 O-δ1	2.4
	Asp-170 O-δ2	2.4
	Gal*p*A[4] O-6A	2.5
	$^{4Ca}Wat^{1}$	2.2

[a] $^{z}Ca^{2+}$ refers to the Z position of the Ca^{2+} ion as defined in Figure 4. $^{x}Wat^{y}$ refers to the Y water molecule associated with either the X Gal*p*A unit or the X Ca^{2+} ion. The labels for the oxygen atoms are defined in Figure 4.

[b] The observed electron density is best suited to a Ca^{2+} with a 50% occupancy rather than to a water molecule. The $^{1}Ca^{2+}$ ion is in the same location, relative to the uronic acid of Gal*p*A[1], as are the other Ca^{2+} ions that coordinate Gal*p*A units. However, unfavorable contact with the well-ordered and fully occupied lysine, Lys-218, was observed. It is not possible to determine whether $^{1}Ca^{2+}$ interacts with an unprotonated lysine at pH 9.5 in the crystals in 50% of the molecules.

occurred between Gal*p*A[3] and Gal*p*A[4]. Moreover, only interactions with Gal*p*A[3] and Gal*p*A[4] involve highly conserved and invariant amino acids within the pectate lyase family. Gal*p*A[3] forms the most protein interactions, which appear to cause the greatest distortion from the 3_1 helical conformation of the tetraGal*p*A. In contrast, there are fewer interactions with Gal*p*A[1] and Gal*p*A[2], and all involve amino acids that are conserved only within the PelC subfamily.

To confirm the position of the scissile glycosidic bond, we investigated the enzymatic cleavage patterns of oligogalacturonates with different degrees of polymerization under optimized assay conditions for PelC. The composition of both the saturated and unsaturated end products was analyzed, and the results, in Table 4, demonstrate that a pentaGal*p*A substrate has two observed modes of binding on PelC. The primary mode yields, as products, an unsaturated trimer (4-en-thrHex*p*A-[Gal*p*A]$_2$) and a saturated dimer at a frequency of 71%. A secondary binding mode occurs at a 29% frequency, yielding an unsaturated dimer (4-en-thrHex*p*A-Gal*p*A) and a saturated trimer. When reduced pentaGal*p*A, containing a galactonic acid at the reducing end, is used as the substrate, the cleavage pattern produces a reduced, unsaturated tetramer ([4-en-thrHex*p*A-Gal*p*A]$_2$-L-Gal-onic, where L-Gal-onic refers to L-galactonic acid) and a saturated monomer at a 68% frequency. In addition, the cleavage pattern produces a reduced, unsaturated trimer (4-en-thrHex*p*A-Gal*p*A-L-Gal-onic) and a saturated dimer at a 32% frequency. The new pattern is indicative of a shift toward the nonreducing end in the position of the scissile bond, because the galactonic acid unit now lies outside the enzyme in the primary binding mode. Because the galactonic acid unit is open rather than in a ring structure, the reduced saccharide cannot participate in the same interactions and occupy the Gal*p*A[1] site on the protein–substrate complex. The only bond position that is consistent with the observed primary-mode cleavage patterns for the reduced and unreduced pentaGal*p*A substrate is that between Gal*p*A[3] and Gal*p*A[4] in the crystals of the protein–substrate complex.

DISCUSSION

The β elimination reaction in pectolytic cleavage is believed to involve three processes: neutralization of the carboxyl group adjacent to the scissile glycosidic bond, abstraction of the C-5 proton, and transfer of the proton to the glycosidic oxygen. In the R218K–$(Ca^{2+})_{3–4}$–pentaGal*p*A structures, the carboxyl group of Gal*p*A[3] is neutralized by interactions with $^{3}Ca^{2+}$ and $^{2}Ca^{2+}$ as well as by Lys-190, an invariant amino acid in the pectate lyase subfamily. Lys-190 also may serve an additional role, which is to partially protonate the carboxylic acid group, stabilizing an enolic intermediate as postulated and defined by Gerlt and colleagues (Gerlt et al., 1991; Gerlt and Gassman, 1992, 1993). Either or both effects serve to decrease the pK_a (the negative log of the dissociation constant) of the α proton at C-5, making it more susceptible to an attack by a base.

It is more difficult to definitively identify the group(s) responsible for proton abstraction and transfer. In our structure, there are no amino acids, water molecules, or Ca^{2+} ions within 3 to 4 Å of any C-5 atom or glycosidic oxygen for any Gal*p*A unit. If the wild-type PelC structure is superimposed upon the R218K–substrate structure, as shown in Figure 5, there are minimal changes in the conformation of any side chain. However, one guanidinium nitrogen of the wild-type amino acid Arg-218 is positioned within 2.6 Å of C-5 of Gal*p*A[3], and the other nitrogen, at a distance of 2.7 Å, interacts with an oxygen of the carboxyl group. The latter in-

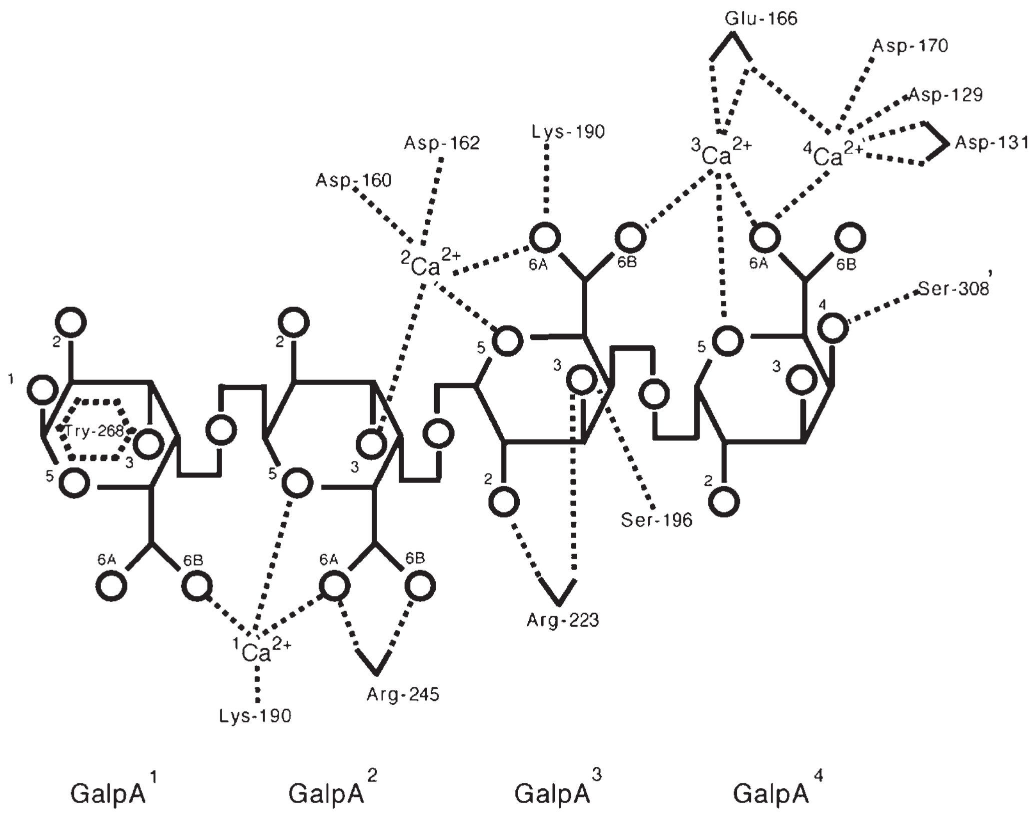

Figure 4. Schematic Representation of R218K and Ca^{2+} Ion Interactions with TetraGal*p*A at a Distance of ⩽3.0 Å.

Gal*p*A[1] is the reducing saccharide, and Gal*p*A[4] is the nonreducing terminus. The interactions are designated with dotted lines, and the distances are given in Table 4. Oxygen atoms are represented by circles, with the corresponding number, and the carbon atoms are assumed at the intersection of bonds designated in boldface lines. Water molecules, which interact with tetraGal*p*A, are not shown but are listed in Table 4.

teraction is likely to be responsible for the lowered pK_a calculated for Arg-218. By using the MEAD program (Bashford and Gerwert, 1992), the calculated pK_a values for all PelC arginine groups, except for Arg-218, fell within the range of 12.0 to 12.5. In contrast, the calculated pK_a value for Arg-218 is 9.5, approximately the same as the pH optimum of the reaction. It is highly unusual for an arginine to act as a general base during catalysis. However, as the H285R mutant of the acyl–acyl carrier protein thioesterase illustrates (Yuan et al., 1995), it is not impossible. The site-specific mutation of the catalytic histidine to an arginine shifts the enzymatic pH optimum from 8.5 to 12. In PelC, the orientation of Arg-218 suggests a catalytic role, which is consistent with other known data, including the high pH optima for all pectate lyase–catalyzed reactions in vitro, the catalytic impairment of the R218K mutation, and the invariance of a comparable arginine in the pectate lyase superfamily.

In the structures presented in this study, no alternative atoms are close enough to the glycosidic oxygen between Gal*p*A[3] and Gal*p*A[4] to serve as a proton donor. When a partially flattened Gal*p*A[3] ring, expected during a β elimination reaction, is modeled, a water molecule lies within 3 to 4 Å of the glycosidic oxygen. The same water molecule, designated as ^{3Ca}Wat[2], coordinates strongly to $^{3}Ca^{2+}$ and possibly is activated by the Ca^{2+} ion. Additional experiments are underway to test the novel enzymatic mechanism implied by the structural results.

In summary, the structures of the R218K–$(Ca^{2+})_{3–4}$–pentaGal*p*A complexes provide an atomic view of a pectate component of the plant cell wall, revealing a right-handed, mixed 2_1 and 3_1 helical conformation for the observed tetraGal*p*A fragment and unanticipated Ca^{2+} positions. The complex represents a Michaelis complex in the reaction pathway, and the details have led to a possible catalytic mechanism, involving a novel role for an arginine as a C-5 proton abstractor. Moreover, the structure provides a functional explanation for all of the invariant and conserved residues in the pectolytic active site region of the pectate lyases. Unfortunately, the structure does not provide an explanation for another set of invariant residues, the vWiDH amino acid sequence, located in a second putative active site (Henrissat et al., 1996), but one that is too small to accommodate long

Table 4. End Product Analyses of PelC Cleavage of Oligogalacturonates

Oligomer Substrate[a]	Products[b]	Frequency (%)	Rate (μkat/mg)
$(\mathrm{Gal}p\mathrm{A})_3$	Gal*p*A + 4-en-thrHex*p*A-Gal*p*A	100	0.17
$(\mathrm{Gal}p\mathrm{A})_4$	Gal*p*A + 4-en-thrHex*p*A-$(\mathrm{Gal}p\mathrm{A})_2$	25	3 to 4
	$(\mathrm{Gal}p\mathrm{A})_2$ + 4-en-thrHex*p*A-Gal*p*A	75	
$(\mathrm{Gal}p\mathrm{A})_5$	$(\mathrm{Gal}p\mathrm{A})_2$ + 4-en-thrHex*p*A-$(\mathrm{Gal}p\mathrm{A})_2$	71	10.1
	$(\mathrm{Gal}p\mathrm{A})_3$ + 4-en-thrHex*p*A-Gal*p*A	29	
$(\mathrm{Gal}p\mathrm{A})_6$	$(\mathrm{Gal}p\mathrm{A})_2$ + 4-en-thrHex*p*A-$(\mathrm{Gal}p\mathrm{A})_3$	9	16.1
	$(\mathrm{Gal}p\mathrm{A})_3$ + 4-en-thrHex*p*A-$(\mathrm{Gal}p\mathrm{A})_2$	53	
	$(\mathrm{Gal}p\mathrm{A})_4$ + 4-en-thrHex*p*A-Gal*p*A	38	
$(\mathrm{Gal}p\mathrm{A})_7$	$(\mathrm{Gal}p\mathrm{A})_2$ + 4-en-thrHex*p*A-$(\mathrm{Gal}p\mathrm{A})_4$	4	22.7
	$(\mathrm{Gal}p\mathrm{A})_3$ + 4-en-thrHex*p*A-$(\mathrm{Gal}p\mathrm{A})_3$	9	
	$(\mathrm{Gal}p\mathrm{A})_4$ + 4-en-thrHex*p*A-$(\mathrm{Gal}p\mathrm{A})_2$	55	
	$(\mathrm{Gal}p\mathrm{A})_5$ + 4-en-thrHex*p*A-Gal*p*A	32	
L-Gal-onic-$(\mathrm{Gal}p\mathrm{A})_2$	No cleavage	0	
L-Gal-onic-$(\mathrm{Gal}p\mathrm{A})_3$	Gal*p*A + 4-en-thrHex*p*A-Gal*p*A-L-Gal-onic	100	0.1
L-Gal-onic-$(\mathrm{Gal}p\mathrm{A})_4$	$(\mathrm{Gal}p\mathrm{A})_2$ + 4-en-thrHex*p*A-Gal*p*A-L-Gal-onic	32	1.2
	Gal*p*A + 4-en-thrHex*p*A-$(\mathrm{Gal}p\mathrm{A})_2$-L-Gal-onic	68	
L-Gal-onic-$(\mathrm{Gal}p\mathrm{A})_5$	$(\mathrm{Gal}p\mathrm{A})_4$ + 4-en-thrHex*p*A-L-Gal-onic	2	4.0
	$(\mathrm{Gal}p\mathrm{A})_3$ + 4-en-thrHex*p*A-Gal*p*A-L-Gal-onic	16	
	$(\mathrm{Gal}p\mathrm{A})_2$ + 4-en-thrHex*p*A-$(\mathrm{Gal}p\mathrm{A})_2$-L-Gal-onic	82	
L-Gal-onic-$(\mathrm{Gal}p\mathrm{A})_6$	$(\mathrm{Gal}p\mathrm{A})_5$ + 4-en-thrHex*p*A-L-Gal-onic	8	4.0
	$(\mathrm{Gal}p\mathrm{A})_4$ + 4-en-thrHex*p*A-Gal*p*A-L-Gal-onic	21	
	$(\mathrm{Gal}p\mathrm{A})_3$ + 4-en-thrHex*p*A-$(\mathrm{Gal}p\mathrm{A})_2$-L-Gal-onic	66	
	$(\mathrm{Gal}p\mathrm{A})_2$ + 4-en-thrHex*p*A-$(\mathrm{Gal}p\mathrm{A})_3$-L-Gal-onic	5	

[a] L-Gal-onic refers to L-galactonic acid or the reduced form of galacturonic acid.
[b] 4-En-thrHex*p*A refers to α-L-eno-threohexosylpyranosyluronic acid or the 4,5-unsaturated form of galacturonic acid.

oligosaccharides. Despite the solvent accessibility in the crystals, no Gal*p*A units are found near the vWiDH region, eliminating the possibility that the invariant amino acids are involved in pectolytic activity.

METHODS

Preparation of Oligogalacturonates and Analyses of Reaction Products

Oligogalacturonates with two to seven Gal*p*A units were prepared from polygalacturonic acid (PGA), as described previously (Kester and Visser, 1990). Reduced oligogalacturonates were prepared according to the method of Omran et al. (1986). Quantitation of the oligomers and analyses of the reaction products were conducted as described previously (Parenicova et al., 1998). Enzymatic reaction rates for oligogalacturonates with different degrees of polymerization were determined spectrophotometrically at 235 nm by using 0.5 mM oligogalacturonate in 0.1 M 2-amino-2-methyl-1-propanol buffer, pH 9.5, in the presence of 1.0 mM $CaCl_2$ at 25°C. Enzyme activities were expressed as μkat/mg by using the molar extinction coefficient at 235 nm for unsaturated digalacturonate of 4600 M^{-1} cm^{-1} at pH 8.0 (MacMillan and Vaughn, 1964). For the determination of bond cleavage frequencies, enzyme reactions were performed using the same reaction conditions, except that the buffer strength was lowered to 20 mM to prevent buffer component interference in the chromatographic analysis. Aliquots were taken at timed intervals, and the reactions were stopped by lowering the pH to 4.5 by the addition of 0.1 volume 1% acetic acid. Reaction products were analyzed as described previously (Hotchkiss et al., 1991; Hotchkiss and Hicks, 1993; Lieker et al., 1993; Benen et al., 1996) by using a Dionex BioLC high-performance chromatography system (Sunnyvale, CA). Detection was done by pulsed amperometry and spectrophotometry at 235 nm. Quantitation of the saturated reaction products was done using the amperometric data and the amperometric response of a calibration mixture of oligogalacturonates with different degrees of polymerization. The unsaturated oligogalacturonates were quantitated using the spectrophotometric response.

A fast-atom bombardment mass spectrum of pentaGal*p*A displayed the major difference between the molecular ion and hydrogen, $(M\text{-}H)^-$, at a mass-to-charge ratio (m/z) of 897.6. Relatively minor amounts of $(M\text{-}H)^-$ ions at m/z ratios of 721.5, 545.4, and 369.3 also were detected, representing tetraGal*p*A, triGal*p*A, and diGal*p*A, respectively. Mass spectra were obtained with a ZAB 2-SE high-field magnetic sector mass spectrometer (VG Analytical,

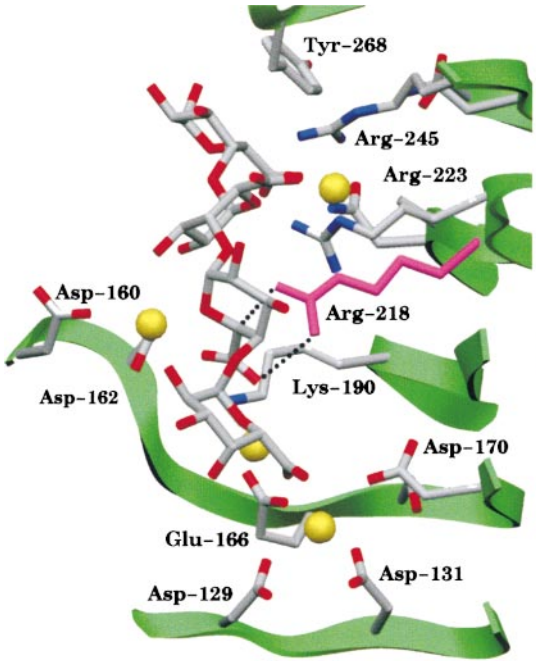

Figure 5. Stereoview of the $(Ca^{2+})_4$–TetraGal*p*A Substrate Superimposed upon the Structure of Wild-Type PelC.

The color scheme is the same as that used in Figure 1, except that wild-type Arg-218 is present and highlighted in magenta. One of the guanidinium nitrogens of Arg-218 lies within 2.6 Å of C-5 of Gal*p*A[3], and the other nitrogen lies within 2.7 Å of O-6B of Gal*p*A[3].

Manchester, UK) by using a cesium gun for fast-atom bombardment ionization at 8000 electron volts, glycerol–thioglycerol–triethylamine (10:10:1) as the matrix, and cesium iodide for mass calibration. The pentaGal*p*A sample was dissolved in water.

Preparation of Crystals

The R218K mutant of pectate lyase C (PelC) was isolated from the periplasm of *Escherichia coli* HMS174(DE3) cells harboring pRSET5A constructs and purified as previously described (Kita et al., 1996). Crystals were grown using conditions similar to that for wild-type PelC crystals (Yoder et al., 1990). The R218K mutant crystals are isomorphous with wild-type PelC crystals and belong to space group $P2_12_12_1$ with unit cell parameters of $a = 72.14$ Å, $b = 78.32$ Å, and $c = 94.43$ Å, with one molecule per asymmetric unit. The R218K crystals were transferred from ammonium sulfate to a solution at pH 9.5 containing cryogenic agents, 7 mM Ca^{2+}, and 50 mM pentaGal*p*A, and after 30 hr, they were frozen in liquid nitrogen for data collection.

X-Ray Diffraction Data Collection

X-ray diffraction data were collected to a resolution of 2.19 Å at −170°C by using a wavelength of 1.08 Å on a MARS imaging plate detector on Beam-Line 7-1 at the Stanford Synchrotron Radiation Light Source (Stanford, CA). The data were processed using MOSFLM (Leslie, 1996). Data are included in Table 5.

Structure Determination

The structure has been solved by difference Fourier methods. Structure factors, by using the refined PelC model (Yoder and Jurnak, 1995) in which Arg-218 had been omitted, were used to calculate a simulated annealed OMIT electron density map. Before water molecules were positioned, Ca^{2+} ions were fitted into the three highest peaks and refined without restraints. Four Gal*p*A units were fitted to the remaining clustered density with the program O (Jones et al., 1991). The model was refined using the method of slow-cooling simulated annealing as implemented by X-PLOR (Brünger, 1996). The reflection data, with structure factor amplitudes (*F*) greater than two standard deviations, were randomly divided into two sets. The working set was composed of 90% of the data sampled at random, and the test set was composed of the remaining 10% of the data used for cross-validation of the refinement cycles (Brünger, 1993). The parameter and topology files used in X-PLOR were those of Engh and Huber (1991) for the protein and those of Ha et al. (1988), as modified by Weis et al. (1990), for the saccharide.

The conformation of each amino acid in the substrate binding region was adjusted by a series of refined OMIT maps in which a region of 8 Å around a residue had been omitted from the structure factor calculations and refinement (Hodel et al., 1992). In subsequent difference maps, peaks $>4\sigma$ and satisfying reasonable distance and geometry criteria were assigned as water molecules by using MAPMAN (Kleywegt and Jones, 1996). All water molecules were inspected visually. In one location, a water molecule could not account adequately for the residual electron density. Because the density was

Table 5. Crystallographic Data Collection and Refinement Statistics for the PelC R218K–$(Ca^{2+})_{3-4}$–PentaGal*p*A Complexes

Parameter	Value
Resolution	2.2Å
Total observations	93,630
Unique observations	27,518
Percent completeness	95.1%
Average I/σ	11.8
R_{sym}[a]	3.1%
Resolution range of refinement	2.2 to 10.0 Å
No. of reflections with $F > 2\sigma$	26,662
Nonhydrogen protein atoms/asymmetric unit	2,647
Water molecules/asymmetric unit	328
Ca^{2+} molecules/asymmetric unit[b]	3 to 4
Gal*p*A molecules/asymmetric unit	4
R_{test}[c] for 10% data	23.3
R_{work}[d] for 90% data	18.6
Root-mean-square deviation from ideal geometry	
Bond length	0.0006 Å
Bond angle	1.54°
Impropers	1.17°
Average thermal factors	
Main chain	9.6 $Å^2$
Side chain	10.0 $Å^2$
All protein atoms	9.7 $Å^2$
Water molecules	22.6 $Å^2$
All nonhydrogen atoms	11.1 $Å^2$

[a] $R_{sym} = 100 = \Sigma|I\text{avg} - I\text{obs}|/\Sigma I_{avg}$, when I_{avg} is the average (avg) or the observed (obs) intensity of the reflection.
[b] Three of the Ca^{2+} ions refined to a 100% occupancy, and the fourth Ca^{2+} ion refined to a 50% occupancy.
[c] $R_{test} = \Sigma|F_o - Fc|/\Sigma|Fc|$ for the 10% of the reflections that were set aside for cross-validation and not used in the refinement.
[d] $R_{work} = \Sigma|F_o - Fc|/\Sigma|Fc|$ for the 90% of the reflections used in the refinement calculations.

located near to the carboxyl group of Gal*p*A[1], in the same relative location as the other Ca^{2+} ions to the coordinating Gal*p*A units, the density was assigned as a fourth Ca^{2+} ion, $^1Ca^{2+}$, with a lowered occupancy. After several cycles of refinements, the best fit of the density appeared to be that for a Ca^{2+} ion with 50% occupancy and a thermal factor of 15 $Å^2$. However, with this assignment, there remains an unfavorable contact with a well-ordered and fully occupied lysine, Lys-218. It is not possible to determine whether $^1Ca^{2+}$ interacts with an unprotonated lysine at pH 9.5 in the crystals in 50% of the molecules.

The final atomic model consists of 352 amino acids, 328 water molecules, 3.5 Ca^{2+} ions, and an α-1,4–linked oligosaccharide consisting of four well-ordered Gal*p*A units. The final model refined to a crystallographic *R* factor of 18.6% for all measured reflections with structure–factor amplitudes $F > 2\sigma$ in the 2.2 to 10.0 Å range. For the final statistics calculations, all reflections $>2\sigma$ were used, including the test data set. The model was checked throughout using PROCHECK (Laskowski et al., 1993), and with the exception of the Lys-218–$^1Ca^{2+}$ distance, no bad contacts were observed in the final model. Refinement statistics are summarized in Table 5. All model figures were prepared using SETOR (Evans, 1993).

Estimation of pK_a Values

The pK_a values for individual amino acids within the three-dimensional structure of the R218K–$(Ca^{2+})_{3-4}$–Gal*p*A_5 complexes were determined using macroscopic electrostatics with atomic detail (MEAD), version 1.1.8 (Bashford and Gerwert, 1992). Standard partial atom charges were used, and the intrinsic pK_a values were calculated from the MEAD program multiflex.

ACKNOWLEDGMENTS

The research was supported by the U.S. Department of Agriculture (Grant No. 96-02966 to F.J.), the National Science Foundation (Grant No. MCB9408999 to N.T.K. and F.J.), and the San Diego Supercomputer Center. The research was conducted in part at the Stanford Synchrotron Radiation Laboratory, which is operated by the Office of Basic Energy Science of the U.S. Department of Energy.

Received August 10, 1998; accepted March 28, 1999.

REFERENCES

Atkins, E.D.T., Nieduszynski, I.A., Mackie, W., Parker, K.D., and Smolko, E.E. (1973). Structural components of alginic acid. II. The crystalline structure of poly-α-guluronic acid. Results of x-ray diffraction and polarized infrared studies. Biopolymers **12,** 1879–1887.

Barras, F., Van Gijsegem, F., and Chatterjee, A.K. (1994). Extracellular enzymes and pathogenesis of soft rot *Erwinia.* Annu. Rev. Phytopathol. **32,** 201–234.

Bashford, D., and Gerwert, K. (1992). Electrostatic calculations of the pK_a values of ionizable groups in bacteriorhodopsin. J. Mol. Biol. **224,** 473–486.

Benen, J.A.E., Kester, H.C.M., Parenicova, L., and Visser, J. (1996). Kinetics and mode of action of *Aspergillus niger* polygalacturonase. In Progress in Biotechnology: Pectins and Pectinases, Vol. 14, J. Visser and A.G.J. Voragen, eds (Amsterdam: Elsevier), pp. 221–230.

Brünger, A.T. (1993). Assessment of phase accuracy by cross validation: The free *R* value. Methods and applications. Acta Crystallogr. **D49,** 24–36.

Brünger, A.T. (1996). X-PLOR Manual, Version 3.8. (New Haven, CT: Yale University).

Carpita, N.C., and Gibeaut, D.M. (1993). Structural models of primary cell walls in flowering plants—Consistency of molecular structure with the physical properties of the walls during growth. Plant J. **3,** 1–30.

Catoire, L., Derouet, C., Redon, A.M., Goldberg, R., and Dupenhoat, C.H. (1997). An NMR study of the dynamic single-stranded conformation of sodium pectate. Carbohydr. Res. **9,** 19–29.

Collmer, A., and Keen, N.T. (1986). The role of pectic enzymes in plant pathogenesis. Annu. Rev. Phytopathol. **24,** 383–409.

DiNola, A., Fabrizi, G., Lamba, D., and Segre, A.L. (1994). Solution conformation of a pectic acid fragment by ^{1}H-NMR and molecular dynamics. Biopolymers **34,** 457–462.

Engh, R.A., and Huber, R. (1991). Accurate bond and angle parameters for x-ray protein structure refinement. Acta Crystallogr. **A47,** 392–400.

Evans, S.V. (1993). SETOR. J. Mol. Graphics **11,** 134.

Gerlt, J.A., and Gassman, P.G. (1992). Understanding enzyme-catalyzed proton abstraction from carbon acids: Details of stepwise mechanism for β-elimination reactions. J. Am. Chem. Soc. **114,** 5928–5934.

Gerlt, J.A., and Gassman, P.G. (1993). An explanation for rapid enzyme-catalyzed proton abstraction from carbon acids: Importance of late transition states in concerted mechanisms. J. Am. Chem. Soc. **115,** 11552–11568.

Gerlt, J.A., Kozarich, J.W., Kenyon, G.L., and Gassman, P.G. (1991). Electrophilic catalysis can explain the unexpected acidity of carbon acids in enzyme catalyzed reactions. J. Am. Chem. Soc. **113,** 9667–9669.

Gouvion, C., Mazeau, K., Heyraud, A., Taravel, F.R., and Tvaroska, I. (1994). Conformational study of digalacturonic acid and sodium digalacturonate in solution. Carbohydr. Res. **261,** 187–202.

Grant, G.T., Morris, E.R., Rees, D.A., Smith, P.J.C., and Thom, D. (1973). Biological interactions between polysaccharides and divalent cations. FEBS Lett. **32,** 195–198.

Ha, S.N., Giammona, A., Field, M., and Brady, J.W. (1988). A revised potential energy surface for molecular mechanic studies of carbohydrates. Carbohydr. Res. **180,** 207–221.

Henrissat, B., Heffron, S.E., Yoder, M.D., Lietzke, S.E., and Jurnak, F. (1996). Functional implications of structure-based sequence alignment of proteins in the extracellular pectate lyase superfamily. Plant Physiol. **107,** 963–976.

Hodel, A., Kim, S.H., and Brünger, A.T. (1992). Model bias in macromolecular crystal structures. Acta Crystallogr. **A48,** 851–858.

Hotchkiss, A.T., and Hicks, K.B. (1993). Analysis of pectate lyase-generated oligogalacturonic acids by high-performance anion-exchange chromatography with pulsed amperometric detection. Carbohydr. Res. **247,** 1–7.

Hotchkiss, A.T., Hicks, K.B., Doner, L.W., and Irwin, P.L. (1991). Isolation of oligogalacturonic acids in gram quantities by preparative HPLC. Carbohydr. Res. **215,** 81–90.

Hricovini, M., Slavomir, B., and Malovikova, A. (1991). Conformations of (1→4)-linked α-D-galacturono-di- and -tri-saccharides in solution analyzed by n.m.r. measurements and theoretical calculations. Carbohydr. Res. **220,** 23–31.

Jarvis, M.C., and Apperley, D.C. (1995). Chain conformation in concentrated pectic gels: Evidence from ^{13}C-NMR. Carbohydr. Res. **275,** 131–145.

Jones, T.A., Zou, J.-Y., Cowan, S.W., and Kjeldgaard, M. (1991). Improved methods for building protein models in electron density maps and the location of errors in these models. Acta Crystallogr. **A47,** 110–119.

Kester, H.C.M., and Visser, J. (1990). Purification and characterization of polygalacturonases produced by the fungus *Aspergillus niger.* Biotechnol. Appl. Biochem. **12,** 150–160.

Kita, N., Boyd, C.M., Garrett, M.R., Jurnak, F., and Keen, N.T. (1996). Differential effect of site-directed mutations in PelC of pectate lyase activity, plant tissue maceration, and elicitor activity. J. Biol. Chem. **271,** 26529–26535.

Kleywegt, G.T., and Jones, T.A. (1996). Biomacromolecular XDL Mapman and XDL Dataman—Programs for reformatting, analysis and manipulation of electron density maps. Acta Crystallogr. **D52,** 826–828.

Kohn, R. (1975). Ion binding on polyuronates—Alginate and pectin. Pure Appl. Chem. **42,** 371–397.

Kotoujansky, A. (1987). Molecular genetics of soft rot *Erwinia*s. Annu. Rev. Phytopathol. **25,** 405–430.

Laskowski, R.A., McArthur, M.W., Moss, D.S., and Thornton, J.M. (1993). PROCHECK: A program to check the stereochemical quality of protein structures. J. Appl. Crystallogr. **26,** 283–291.

Leslie, A.G.W. (1996). MOSFLM User Guide. (Cambridge, UK: Medical Research Council Laboratory of Molecular Biology).

Lieker, H.-P., Thielecke, K., Buchholz, K., and Reilly, P.J. (1993). High performance anion-exchange chromatography of saturated and unsaturated oligogalacturonic acids. Carbohydr. Res. **238,** 307–311.

Lietzke, S.E., Keen, N.T., Yoder, M.D., and Jurnak, F. (1994). The three-dimensional structure of pectate lyase E, a plant virulence factor from *Erwinia chrysanthemi.* Plant Physiol. **106,** 849–862.

MacMillan, J.D., and Vaughn, R.H. (1964). Purification and properties of a polygalacturonic acid *trans*-eliminase produced by *Clostridium multifermentans.* Biochemistry **3,** 564–572.

Mayans, O., Scott, M., Connerton, I., Gravesen, T., Benen, J., Visser, J., Pickersgill, R., and Jenkins, J. (1997). Two crystal structures of pectin lyase A from *Aspergillus* reveal a pH driven conformational change and striking divergence in the substrate-binding clefts of pectin and pectate lyases. Structure **5,** 677–689.

McNaught, A.D. (1997). Nomenclature of carbohydrates. Adv. Carbohydr. Chem. Biochem. **52,** 43–171.

Morris, E.R., Powell, D.A., Gidley, M.J., and Rees, D.A. (1982). I. Polymorphism between gel and solid states of calcium polygalacturonate. J. Mol. Biol. **155,** 507–516.

Omran, H., Dörreich, K., and Gierscher, K. (1986). Some results of the isolation of discrete enzymes (exopolygalacturonase and pectinesterase) from a commercial pectic enzyme preparation. Lebensm.-Wiss. Technol. **19,** 457–463.

Parenicova, L., Benen, J.A.E., Kester, H.C.M., and Visser, J. (1998). *PgaE* encodes a fourth member of the endopolygalacturonase gene family from *Aspergillus niger.* Eur. J. Biochem. **251,** 72–80.

Pickersgill, R., Jenkins, J., Harris, G., Nasser, W., and Robert-Baudouy, J. (1994). The structure of *Bacillus subtilis* pectate lyase in complex with calcium. Nat. Struct. Biol. **1,** 717–723.

Powell, D.A., Morris, E.R., Gidley, M.J., and Rees, D.A. (1982). Conformations and interactions of pectins. II. Influence of residue sequence on chain association in calcium pectate gels. J. Mol. Biol. **155,** 517–531.

Preston, J.F., Rice, J.D., Ingram, L.O., and Keen, N.T. (1992). Differential depolymerization mechanisms of pectate lyases secreted by *Erwinia chrysanthemi* EC16. J. Bacteriol. **174,** 2039–2042.

Thibault, J.-F., Renard, C.M.G.C., Axelos, M.A.V., Roger, P., and Crepeau, M.-J. (1993). Studies of the length of homogalacturonic regions in pectins by acid hydrolysis. Carbohydr. Res. **238,** 271–286.

Vitali, J., Schick, B., Kester, H.C.M., Visser, J., and Jurnak, F. (1998). The three-dimensional structure of *Aspergillus niger* pectin lyase B at 1.7 angstrom resolution. Plant Physiol. **116,** 69–80.

Walkinshaw, M.D., and Arnott, S. (1981a). Conformations and interactions of pectins. I. X-ray diffraction analysis of sodium pectate in neutral acidified forms. J. Mol. Biol. **153,** 1055–1073.

Walkinshaw, M.D., and Arnott, S. (1981b). Conformations and interactions of pectins. II. Models of junction zones in pectinic acid and calcium pectate gels. J. Mol. Biol. **153,** 1075–1085.

Weis, W.I., Brünger, A.T., Skehel, J.J., and Wiley, D.C. (1990). Refinement of the influenza virus hemagglutinin by simulated annealing. J. Mol. Biol. **212,** 737–761.

Yoder, M.D., and Jurnak, F. (1995). The refined three-dimensional structure of pectate lyase C from *Erwinia chrysanthemi* at 2.2 Å resolution—Implications for an enzymatic mechanism. Plant Physiol. **107,** 349–364.

Yoder, M.D., DeChaine, D.A., and Jurnak, F. (1990). Preliminary crystallographic analysis of pectate lyase C from *Erwinia chrysanthemi.* J. Biol. Chem. **265,** 11429–11431.

Yoder, M.D., Keen, N.T., and Jurnak, F. (1993). New domain motif: The structure of pectate lyase. Science **260,** 1503–1507.

Yuan, L., Nelson, B.A., and Caryl, G. (1995). The catalytic cysteine and histidine in the plant acyl–acyl carrier protein thioesterases. J. Biol. Chem. **271,** 3417–3419.